

No more Sliding-Windows: dynamic functional connectivity based on random convolutions without learning

Yonjie Duan[†], Zhiying Long^{*}

[†], ^{*}:Beijing Normal University

Abstract

Compared to static functional connectivity, dynamic functional connectivity provides more detailed temporal information. The traditional sliding window method constructs functional connectivity matrices by applying a moving time window across the entire time series to calculate correlations between brain regions. However, as a method of feature extraction, it exhibits significant limitations, such as the dependency of feature dimensions on the window length and the generation of features lacking information from other time points within the window. This paper presents RandCon, a novel method for calculating dynamic functional connectivity (DFC), which employs randomly generated multi-dimensional convolution kernels. This method performs convolution operations directly on the BOLD signal without the need for learning, extracting functional connectivity features. Compared to the sliding window method, RandCon shows notable improvements in performance on simulated data, particularly in terms of temporal accuracy and noise resistance. Results from real data indicate that this method maintains stability within short time windows and better identifies gender differences. Furthermore, we propose a more comprehensive theoretical framework, the multi-dimensional convolution method, where the sliding window method and its variants are specific cases of this method. The proposed method is straightforward and efficient, significantly broadening the scope of dynamic functional connectivity research and offering substantial theoretical and practical potential.

[†]:hg349713171@gmail.com

^{*}:Corresponding author

Introduction

Resting-state functional magnetic resonance imaging (rs-fMRI) is frequently used to investigate the cooperative functioning of various brain regions and to construct functional connectivity networks^{1,2}. Traditional studies have typically assumed that these functional networks are static, analyzing connectivity over entire time periods^{3,4}. However, recent research indicates that the brain's resting state is dynamic, with functional connectivity fluctuating over time^{5,6}. To address this, dynamic functional connectivity (DFC) methods have been developed and have advanced significantly in recent years⁷. Research has shown that the dynamic properties of functional connectivity are intricately linked to processes such as cognition^{8–10}, language^{11–13}, and motor functions^{14,15}. Furthermore, alterations in brain dynamics have been identified in several psychiatric and cognitive disorders, including schizophrenia¹⁶, attention deficit hyperactivity disorder (ADHD)^{17,18}, and autism^{16,19}.

In the research methodologies pertaining to dynamic functional connectivity, including time-frequency analysis^{4,20,21}, Hidden Markov Model method^{22–24}, Multiplication of Temporal Derivatives (MTD)²⁵ and other data-driven models^{26–28}, the sliding window approach remains the most classical and widely used method^{3,5,6,20,29,30}. DFC based on sliding window firstly applies a moving time window across the entire time series. Then, the functional correlation connectivity matrix of regions of interests (ROI) is calculated within each window. Finally, clustering method is applied to identify the intrinsic "states" that repetitively occur over time²⁰. Despite its successes, the sliding window method faces significant challenges^{5,31,32}. Hindriks³¹ found that traditional sliding window methods fail to detect dynamic functional connectivity in individual subjects. Other studies have noted that shorter window lengths can lead to an increase in false signals, while longer window lengths reduce the ability to capture rapid dynamics^{32,33}.

In recent years, several studies have aimed to refine the sliding window method to improve its capacity for detecting brain dynamics and enhancing interpretability. Leonardi³² recommended using a longer time window to ensure reliable dynamic connectivity detection. Zhuang et al.³⁴ employed the frequency at each time point to determine the sliding window length, thereby capturing the temporal dynamics in fMRI data more accurately. Espinoza et al.³⁵ proposed a novel sliding window method that includes first-order derivatives of DFC to more accurately characterize whole-brain functional connectivity variations over time, more accurately highlighting group differences between healthy controls (HC) and schizophrenia patients (SZ) across different connectivity states. Vergara et al.³⁶ proposes Average Sliding Window Correlation (ASWC) method, which significantly reduces artifacts and improves temporal resolution by using shorter window lengths and averaging techniques compared to the traditional Sliding Window method. Mokhtari²⁹ proposed a modulation rectangular window to resolve the issue of high-frequency dynamic correlation suppression caused by spectral non-uniformity in sliding window correlation analysis. By employing a flat spectrum design, this method enhances the capability to capture rapid dynamic correlations and detect network state transitions.

For the DFC of sliding windows, each window extracts features from each ROI, allowing functional connectivity to be obtained by calculating the correlation of features between pairs of ROIs. In each sliding window, the signal amplitude at each time point is considered an extracted feature, with the number of features equaling the window length. A small number of features (short window length) cannot effectively capture true functional connectivity between ROIs, whereas a

large number of features (long window length) fails to capture rapid time-varying changes in brain dynamics. If sufficient features can be extracted from each ROI independent of window length, functional connectivity between ROIs can be achieved even with a small window length. Therefore, it is crucial to investigate methods for effectively extracting sufficient features from each ROI's signal without relying on window length. Additionally, this feature extraction method presents another issue: each extracted feature corresponds only to the information of a single time point in the original signal. The traditional sliding window method uses the BOLD signal value at a single time point as a feature directly, whereas some variations of this method^{29,36} employ the weighted original signal as the feature. Both approaches neglect a key characteristic of the BOLD signal, which is the continuity and correlation between BOLD signal values at adjacent time points. Integrating information from multiple time points into each extracted feature could yield more meaningful features.

Convolution has been widely applied to extract local features from signals by sliding a convolution kernel over a signal³⁷. Different kernels can extract different local features by convolving different kernels with the same signal. Thus, the feature number is only dependent on the kernel number rather than the kernel size. Although the convolution kernel is similar to a sliding window, the kernel width doesn't determine the feature number. Equally important is that the convolution method for feature extraction considers not just the signal at a single point but includes information from multiple time points, which is consistent with the characteristics of the BOLD signal. In this study, we propose a multi-dimensional random convolution (RandCon) DFC method that effectively captures time-varying DFC at small time scales. This method avoids both the window size limitation and the information limitation on the features extracted by sliding window method. First, RandCon is applied to extract different local features from each ROI's time series by randomly setting multi-dimensional convolution kernels. Based on these extracted features, the functional connectivity matrix is obtained by calculating the correlation of features between pairs of ROIs. The time-varying functional connectivity matrices are then obtained by sliding the convolution kernel over each ROI's time series. Finally, K-means clustering is applied to all the time-varying functional connectivity matrices to identify intrinsic brain states. By using randomly generated, untrained multi-dimensional convolution kernels, we achieved significantly better results than the sliding window method on simulated data and confirmed its feasibility on real data.

More importantly, we prove that the multi-dimensional convolution method is a general convolution framework that theoretically includes the sliding window method. In this framework, the sliding window method and its variants are special cases of multi-dimensional convolution, with fixed weights in the convolution kernel. The special convolution kernel used in the sliding window method shows significant limitations in window (kernel) size and information capacity. By randomly setting multi-dimensional convolution kernels, these limitations can be removed. Our method pioneers a new domain for dynamic functional connectivity, greatly expanding the exploration space and potential of the method, carrying profound significance.

Results

A. Analysis of Simulated Dataset

Figure 4 includes the results from the first group of subjects, with a noise standard deviation of 0.6, 90 ROIs, 1200 TRs, and a scale parameter of 5. The figure shows the states fitted by the MTD, phase synchronization, sliding window, and RandCon methods, along with their cosine similarity to

the ground truth and the proportion of time spent in each state. It can be seen that, from a temporal perspective, the proportion of time spent in the four states fitted by the RandCon method is the closest to the ground truth, indicating a very high goodness of fit. In terms of spatial similarity, the cosine similarity between the four states fitted by the RandCon model and the ground truth is the highest, demonstrating the best model performance. The following section presents the quantitative results of each sub-experiment.

Robustness Against Noise

In the time dimension, Figure 5(A) presents the ARI values of four different models under varying noise levels. As illustrated, the performance of all models deteriorates as noise variance increases. For each noise level, the MTD method consistently shows the lowest ARI index, with minimal variation as noise increases. The sliding window method and the phase synchronization method produce very similar results, whereas the RandCon method significantly outperforms all others, with statistical testing showing $p < 0.001$, indicating a significant difference.

In the spatial dimension, Figure 5(D) displays the cosine similarity results for the four models under different noise conditions. It is evident that as noise variance increases, the overall cosine similarity of all models decreases, and inter-group differences widen, indicating reduced stability. Unlike the ARI values, the MTD method more accurately fits the ground truth state compared to the sliding window and phase synchronization methods, which continue to yield similar results. Similarly, the cosine similarity values of the RandCon method are higher than those of all other methods and are almost universally significant. For detailed results of the statistical tests in this and subsequent sections, please refer to Supplementary materials.

Robustness to Number of ROIs

In the time dimension, Figure 5(B) presents the ARI values of four models as the number of ROIs increases. The results show a general improvement in performance for almost all models with an increasing number of ROIs. The MTD method consistently has the lowest ARI values and exhibits a slow rate of improvement. The sliding window method and phase synchronization method show similar and modest improvement trends. In contrast, the RandCon method demonstrates a clear and significant improvement, with the model's stability markedly increasing as the total number of ROIs grows. For every number of ROIs, the RandCon model's results are significantly higher than those of the other three models.

In the spatial dimension, Figure 5(E) illustrates the cosine similarity results for the four models across different numbers of ROIs. When the number of ROIs is low, all four methods show relatively high and similar results. However, as the number of ROIs increases, the performance of the RandCon model stabilizes and significantly exceeds the results of the other three models.

Robustness to Number of TRs

Figure 5(C) presents the ARI values of four models across different numbers of TRs, highlighting temporal differences. With an increasing number of TRs, the performance of the RandCon model improves steadily, and its stability also enhances. The MTD method consistently shows the lowest ARI values in the time dimension, while the sliding window method and phase synchronization method remain similar. Across all scenarios, the RandCon model significantly outperforms the other three models.

In the spatial dimension, Figure 5(F) illustrates the cosine similarity results. When the TR value is

low, all four models yield similar results. However, as the TR value increases, the RandCon model's stability improves significantly, resulting in higher performance compared to the other three models.

Robustness to Number of Latent States

Figure 6(A) presents the time dimension results of four models with varying numbers of hidden states. As the number of hidden states increases, the performance of the RandCon model declines, and its stability decreases. The MTD method is largely unaffected by changes in the number of hidden states. For the sliding window and phase synchronization methods, while their average performance improves with an increasing number of states, their stability diminishes. Across all numbers of hidden states, the RandCon method consistently outperforms the other three methods significantly.

In the spatial dimension, Figure 6(D) shows that changes in the number of hidden states have minimal impact on the performance of each model, with their results being relatively similar. Nonetheless, the RandCon model still significantly outperforms all other models.

Robustness to State Transition Frequency

According to Figure 6(B), in the time dimension, similar to previous observations, when the scale parameter is 5, which is the standard setting, the RandCon model achieves the best performance and the highest stability. For the MTD, sliding window, and phase synchronization methods, as the scale parameter increases, their performance gradually improves, but the rate of improvement is slow. Across all scale parameters, the RandCon method significantly outperforms the other models.

In the spatial dimension, Figure 6(E) shows that the results of the four models are quite similar. The RandCon model has the highest mean performance, followed by the MTD method, with the sliding window and phase synchronization methods performing similarly. When the scale parameter is 1, RandCon is only significantly better than the sliding window method. In all other cases, RandCon significantly outperforms all other models.

Evaluation of The Number of Convolution Kernels

Figure 6(C) illustrates the effect of varying the number of convolutional kernels on ARI results under different noise conditions. As shown, the overall performance of the models decreases as noise levels increase. However, within each noise condition, model performance improves with an increasing number of convolutional kernels, indicating that more kernels enhance feature extraction and noise resistance. When the noise level is low (e.g., 0.6), model performance stabilizes after reaching 20 convolutional kernels. In contrast, at a high noise level (e.g., 2.1), model performance continues to improve with additional kernels, suggesting that higher noise levels require more convolutional kernels to achieve peak performance.

In the spatial dimension, Figure 6(F) reveals a similar pattern: high noise levels reduce model performance, while more convolutional kernels boost it. Compared to the time dimension, it is more apparent that under high noise conditions, increasing the number of convolutional kernels consistently enhances model performance. Conversely, under low noise conditions, the model's performance plateaus once a certain number of convolutional kernels is reached.

Evaluation of The Size of Convolution Kernels

Figure 7 compares the sliding window method and the RandCon method using different

convolutional kernel shapes. Measured by Sojourn Time, the data show that as both the convolutional kernel length and window length increase, overall KL divergence decreases and accuracy improves, indicating a Sojourn Time closer to the correct sequence. In all tested lengths, the RandCon model outperforms the sliding window method, proving its effectiveness beyond the 1×3 convolutional kernel shape.

However, because the convolutional kernel parameters are randomized, longer kernels involve more time points, diluting the impact of this randomness. Thus, with shorter convolutional kernels, the RandCon model's performance advantage is pronounced, but as the kernel length increases, its results begin to converge with those of the sliding window method. Specifically, for kernel lengths between 4 and 8, the RandCon model significantly outperforms the sliding window method. At a kernel length of 9, however, the performance difference is no longer significant.

From the spatial dimension, considering metrics such as cosine similarity and MSE, the results are similar to those observed in the temporal dimension. As the convolution kernel size and window length increase, the model's spatial fitting accuracy improves, indicated by higher cosine similarity and lower MSE. For each window length, the RandCon method outperforms the sliding window method. Specifically, when the window length is 8, the performance of RandCon in terms of cosine similarity is no longer significantly better, and when the window length is 9, the same applies for MSE.

B. Real Data Analysis

The K-means-Elbow method estimated the optimal number of brain states to be 4. Figure 8 illustrates the functional connectivity (FC) patterns of the four intrinsic brain states identified using RandCon and the sliding windows methods. The patterns observed for the four brain states were similar across both methods. Among these states, state 3 exhibited generally weak connections, while state 4 exhibited generally strong connections.

Temporal and spatial DFC analysis for Sliding windows and RandCon

The temporal DFC results for the two methods, including the fraction of time and the mean dwell time for each brain state, are presented in Figure 9. Firstly, for the fraction of time metric, the sliding windows method did not detect any significant gender differences across all states showed in Figure 9(D). In state 1, the average proportion of time spent by male subjects was slightly higher than that of female subjects, but this difference was not statistically significant. Conversely, the RandCon method found that in state 1, the proportion of time spent by male subjects was significantly lower than that of female subjects (Figure 9(A)). For the other three states, both methods produced similar results, with consistent average gender differences.

Regarding the mean dwell time, the RandCon method showed higher average dwell times for each state compared to the sliding windows method, which may suggest that the RandCon method offers better stability within shorter time windows and convolution kernel lengths. In terms of intergroup differences, both methods detected similar results. As illustrated in Figure 9(E), the sliding windows method found that male subjects exhibited significantly higher dwell times in state 2 compared to female subjects. The RandCon method also observed similar results (Figure 9(B)).

The spatial DFC results for the two methods, including FC Variability and Centroid Similarity for each subject, are presented in Figure 9(C) and 9(F). As shown in Figure, the overall FC Variability index for the RandCon model is lower than that of the sliding windows method. This suggests that with shorter window lengths, the RandCon method maintains relatively stable connectivity matrices,

indicating higher model robustness. For both methods, male subjects exhibited lower average variability than female subjects, with the RandCon method detecting significant differences, while the sliding windows method did not find significant differences.

Regarding the Centroid Similarity metric, Figure 9(C) shows that the overall similarity is higher in the RandCon model. Both methods identified that male subjects have higher similarity than female subjects. The RandCon method detected significant differences in this metric, whereas the sliding windows method did not find significant differences.

Discussion

In this study, we propose a novel method based on random convolution (RandCon), which employs randomly generated multidimensional convolution kernels to extract signal features and compute DFC matrices. Unlike the limitations of the sliding window methods and their variants, the number of features generated by the RandCon method does not depend on the window length, and also, within each extracted feature value, information is integrated from multiple time points. Results from both simulated and real data demonstrate the effectiveness and robustness of this method. Additionally, we introduce a framework for multi-dimensional convolution that incorporates RandCon, sliding window method and the variants of it into the broader theoretical context, significantly enhancing the scalability and flexibility of dynamic functional connectivity methods. In the field of DFC, the sliding window method is the most important and widely used⁷. This method involves extracting signals by taking all signals within a specified time window and calculating the relationship between ROIs or voxels using Pearson correlation. While this method is relatively simple, it introduces several issues. First, there is no gold standard for selecting the window length. A shorter window length increases volatility significantly, while a longer window length fails to capture rapid dynamic changes in the brain⁵. Additionally, this simplified signal extraction approach faces a problem: each feature value corresponds to the signal at only one time point, which neglects the characteristic of BOLD signals that adjacent time points have mutual influence and continuity. Some studies have proposed improvements to the sliding window method, such as using different window shapes²⁹ (essentially applying fixed weights to the time points within the window) or using signal transformation techniques to determine the optimal window size³⁴, etc. However, these improvements do not overcome the fundamental limitations of the sliding window method, and therefore, the mentioned two fundamental problems remain unresolved.

Convolution, as a method of signal extraction, is a fundamental operation³⁷. Through local connections and shared parameters, it effectively extracts local features and spatiotemporal relationships from images or other data, enabling filtering, smoothing, enhancing, and denoising. This technique has broad applications across various fields. In signal processing, convolution is used for filtering and smoothing signals³⁸; in image processing, for image enhancement and edge detection³⁹; in control systems, to describe system responses⁴⁰. Multidimensional convolution employs multiple filters to process input data simultaneously, with each convolution kernel extracting different features. By performing parallel computations with multiple convolution kernels, richer and more diverse feature representations can be obtained. Additionally, by adjusting the number of convolution kernels, the dimensionality of the signal can be changed, achieving dimensionality reduction or augmentation. In summary, convolution holds broad application prospects and significant potential for exploration in the field of DFC.

RandCon, as a type of multidimensional convolution, offers advantages such as computational simplicity and strong stability. It does not require any training; instead, all parameters of the convolution kernels are formed by sampling from a random distribution, greatly enhancing computational speed. Although this method incorporates randomness, it ensures consistency in filtering methods across all times and ROIs for each convolution kernel. Consequently, for two ROIs, despite different dimensions formed by various convolution kernels, the filtering objects, i.e., the BOLD signals of the ROIs, remain consistent. This design aligns with Pearson correlation calculations, enabling RandCon to produce meaningful FC even with random parameters. Additionally, RandCon allows for flexible adjustments in the number of convolution kernels, facilitating changes in feature dimensions. This breaks the constraints of the sliding window method, eliminating the need for a correspondence between feature dimensions and window numbers, thus resolving the issue of window size selection in the sliding window method. Furthermore, unlike the sliding window method, each feature dimension in RandCon is derived from a convolution kernel filtering the original signal. Essentially, each feature dimension encompasses information from all time points within the entire time window, aligning well with the continuous and interrelated nature of BOLD signals, a characteristic not captured by the sliding window method and its variants.

The validation results on the simulated dataset indicate that the RandCon method performs well in the temporal dimension, maintaining stability. As shown in Figures 4 and 5, the model retains better performance in the presence of noise, and its stability significantly improves with an increase in the number of ROIs and TRs, demonstrating clear performance enhancement. Even with variations in the number of hidden states and state transition frequencies, RandCon continues to perform excellently, showcasing robustness to parameter changes. This superior performance is primarily due to RandCon's meaningful feature dimensionality augmentation, which greatly increases the number of features used to calculate DFC, thereby enhancing resistance to noise and other parameter changes. Experiments on model parameters, as seen in Figures 5(C) and 5(F), show that increasing the number of convolution kernels steadily improves model performance, validating the effectiveness of dimensionality augmentation. Additionally, as shown in Figure 7, when the time length increases, within a certain range, RandCon's performance still significantly surpasses that of the sliding window method, indicating that the RandCon model is suitable for both shorter and longer time lengths.

The analysis results on the real dataset further confirm the effectiveness of the RandCon method. By analyzing rs-fMRI data from 100 subjects, RandCon identified brain states similar to those detected by the sliding window method. However, RandCon detected more unique and clearer DFC state patterns compared to the sliding window method (see Figure 8). These more distinct DFC state patterns provide additional insights into understanding each brain state. Thus, these results indirectly support RandCon's superior brain state space detection capability compared to the sliding window method in simulated experiments. Brain states are recurring activity patterns distributed throughout the brain, originating from physiological or cognitive processes. These patterns are neurobiological phenomena correlated with function (e.g., behavior)⁴¹. Brain states have the following characteristics: (1) they are products of specific cognitive or physiological states; (2) they are characterized by widely distributed activity or coupling patterns; and (3) they influence the future physiology and/or behavior of the organism⁴¹. Consequently, we interpreted the cognitive functions of each brain state based on the more unique DFC patterns estimated by RandCon.

For state 1, strong positive correlations are observed between SMN, CON, AUN, VN, and SN, while

connections between DMN, FPN, and SCN are weak, close to zero. SMN serves as an integrator in the brain, processing sensory inputs to form common experiences⁴². CON and SN are involved in the detection and integration of sensory stimuli⁴³, while AUN and VN process auditory and visual inputs. The strong interactions among SMN, CON, AUN, VN, and SN in state 1 suggest that SN detects and integrates auditory/visual stimuli, and SMN oversees responses to these stimuli, forming experiences. Thus, state 1 may be associated with the integration of auditory and visual stimuli and the interpretation of internal and external experiences. In state 2, the overall connection pattern is similar to state 1 but with reduced connection strength, indicating a transition state between state 1 and state 3. The negative connections of the DMN observed in state 1 disappear, replaced by weaker positive connections with networks such as SMN, CON, and AUN, suggesting slight activation of the DMN during this transition. State 3 shows overall weaker connections than other states, with most being negative and close to zero. Such weaker connectivity patterns have been frequently observed in previous studies^{20,44,45} and may be associated with relaxation. For state 4, most connections display strong positive correlations, except for the weak correlations between SCN and other subnetworks. The SCN is crucial for emotional and social functions⁴⁶. The weak connections of SCN with other subnetworks in state 4 may indicate that the subject is engaged in cognitive processes unrelated to emotional or social cognition.

For the DFC analysis of real fMRI data, both RandCon and the sliding window method detected similar group differences in temporal and spatial DFC measurements. However, RandCon identified more group differences in spatial measurements compared to the sliding window method. These results highlight RandCon's advantage in detecting group differences in DFC. We primarily interpret RandCon's results in the analysis of real fMRI data as follows. Compared to the male group, the female group shows a significantly higher proportion of time in state 1 and a significantly lower average dwell time in state 2 (see Figure 9). In contrast, the male group tends to spend more time in state 2 and less time in state 1. This finding is consistent with a previous study that found women spend significantly more time in specific brain states with negative correlations between network systems compared to men⁴⁷. The higher proportion of transition states in the male group may suggest that men experience more information exchange between subnetworks at rest compared to the female group, possibly due to more frequent state switching. From a spatial pattern perspective, the RandCon model found that the central similarity in the male group is significantly higher than in the female group. This indicates that the states of the male group at different times are closer to the average state, suggesting greater state stability in men compared to women. Additionally, in studying FC variability, the male group exhibited significantly lower variability than the female group, indicating that men's states fluctuate and change less over time.

Although the RandCon method has demonstrated excellent performance in DFC analysis, several directions warrant further research. First, integrating deep learning-based methods could enhance RandCon's performance by learning optimal convolution parameters. Secondly, incorporating additional dimensions of signal features, such as frequency characteristics, could improve the model's ability to analyze complex signals. Additionally, it is essential to further validate the applicability of the RandCon method across different types of brain diseases and explore its potential in clinical diagnosis and treatment. In summary, the RandCon method offers a novel perspective for DFC research by effectively overcoming the limitations of traditional sliding window methods through random convolution. Future research can further expand and optimize this approach, potentially bringing significant advancements to neuroimaging and brain science.

Methods

Multi-dimensional Convolution

The flowchart of multi-dimensional convolution is shown in Figure 1. It is assumed that $X \in \mathbb{R}^{N \times T} = (x_1, x_2, \dots, x_N)$ represents a subject's fMRI signal with T time points from N ROIs, where $x_n \in \mathbb{R}^{1 \times T}$ represents the time series of the n -th ROI (see Figure 1(A)). A total of K convolution kernels $\{C_1, C_2, \dots, C_K\}$ are designed to perform convolution on X . Then, the k -th convolution kernel $C_k \in \mathbb{R}^{1 \times W}$ is applied to convolve with the fMRI signal X , ultimately producing a feature signal y_k (see equation 1).

$$y_k(n, t) = \sum_{w=1}^W x_n(t + w - 1) C_k(w) \quad (1)$$

After padding, the dimension of $y_k \in \mathbb{R}^{N \times T}$ keeps consistent with X . After all the K kernels are applied to all the ROI's fMRI signal, the overall output result is $Y = \{y_k(n, t)\} \in \mathbb{R}^{K \times N \times T}$ (Figure 1(B)). Next, we reslice the variable Y based on the temporal dimension to form a time series dataset $Y = \{y_t^*(n, k)\}$, where $y_t^* \in \mathbb{R}^{N \times K}$, representing the K -dimensional features of all N ROIs obtained through multi-dimensional convolution at time point t (Figure 1(C)). Then, for the m -th and n -th ROIs in y_t^* , we use these features to calculate the Pearson correlation coefficient, thereby forming a dynamic functional connectivity matrix Z_t . The formula is as follows:

$$Z_t(n, m) = Z_t(m, n) = \frac{\sum_{k=1}^K (y_t^*(m, k) - \overline{y_t^*(m)})(y_t^*(n, k) - \overline{y_t^*(n)})}{\sqrt{\sum_{k=1}^K (y_t^*(m, k) - \overline{y_t^*(m)})^2} \sqrt{\sum_{k=1}^K (y_t^*(n, k) - \overline{y_t^*(n)})^2}} \quad (2)$$

Where $\overline{y_t^*(m)} = \frac{1}{K} \sum_{k=1}^K y_t^*(m, k)$, $\overline{y_t^*(n)} = \frac{1}{K} \sum_{k=1}^K y_t^*(n, k)$. After calculating the correlation

coefficients, we ultimately obtained $Z = \{Z_1, Z_2, \dots, Z_T\}$, as shown in Figure 1(D). Here,

$Z_t \in \mathbb{R}^{N \times N}$ represents the functional connectivity matrix at time point t . This symmetric matrix has all diagonal values equal to 1, and the value at the m -th row and n -th column corresponds

to the correlation coefficient between ROI m and ROI n at that time point. To remove redundant information, we delete the diagonal values and take only the lower half of the matrix, resulting in a vector of length $\frac{N \times (N-1)}{2}$. We then use K-means clustering on these samples, setting the number of

states to M . Finally, we obtain M cluster centers of $\frac{N \times (N-1)}{2}$ dimensions and a time series of

length T , representing the state of each time point, from 1 to M .

Parameters within the Convolution Kernel

In multi-dimensional convolution methods, it is critical to set proper weight parameters for the convolution kernels. There are three methods to set kernel weights: fixed weights, random sampling, and deep learning methods. In the fixed weight method, the weights of each convolution kernel are manually set to fixed values. This is relatively simple and computationally easy, but the representational power of the extracted features is limited. We proved that the sliding window method is a special case of multi-dimensional convolution with fixed kernel weights. For the deep learning method, the optimal weights are learned from training datasets using deep learning techniques. This method is relatively complex and require extensive training. They are highly dependent on data and are prone to overfitting. In the random sampling method, the weights of each kernel are set by sampling from a probability distribution. The random sampling method, without the need for training, improves the representational capability of features through random sampling and dimensionality augmentation. In all experiments in this paper, the convolution kernel parameters in the RandCon model are determined through random sampling.

Sliding Window Method as a special case of Multi-dimensional Convolution

First, we compare the feature extraction processes of the two methods within a fixed time window or convolution kernel length, without any temporal movement. In the classical sliding window method, assuming the window length is W . For a single ROI within a window, i.e., over W time points, there is a W -length array $X = [x_1, x_2, \dots, x_W] \in \mathbb{R}^{1 \times W}$ where x_w represents the BOLD signal at time point w .

In the multi-dimensional convolution method, a length of time W is also employed as X . For the time series X , K convolution kernels are used $\{C_1, C_2, \dots, C_K\}, C_k \in \mathbb{R}^{1 \times W}$. Each convolution weights and averages all values within X to produce the value:

$$d_k = \sum_{w=1}^W x_w C_k(w) \quad (3)$$

With K kernels, each window produces an array $d = [d_1, d_2, \dots, d_K] \in \mathbb{R}^{1 \times K}$, where each value represents a unique weighted combination of the original data X .

From the perspective of multi-dimensional convolution, the sliding window method can be seen as a special case of fixed parameters type. As depicted in Figure 2, using W convolution kernels

$\{C_1, C_2, \dots, C_W\}, C_w \in \mathbb{R}^{1 \times W}$, where the w -th kernel has a parameter of 1 at the w -th position and 0 elsewhere. After applying these W convolution kernels, the resulting array $d = [d_1, d_2, \dots, d_W] \in \mathbb{R}^{1 \times W}$ matches the sliding window method's output exactly, i.e. $d = X$.

We demonstrated that within a fixed time window, a special multi-dimensional convolution kernel can replace the sliding window method. Furthermore, when both the convolution and sliding window methods use the same stride and padding mode, they yield identical results. Thus, these two methods are entirely equivalent.

When viewed from the multi-dimensional convolution perspective, the sliding window method has two limitations: first, the number of convolution kernels must equal the total number of time points in the window; second, each kernel must have a single value of 1 with all other values being 0. This results in a fixed number of features, each containing information from only one time point, significantly limiting expressive capability. Many enhancements to the sliding window method have not overcome these limitations, differing only in that each convolution kernel's value may not be 1 but another weight. Consequently, the multi-dimensional Convolution method holds substantial potential and exploratory space, warranting further attention and research.

Experiment

A. Analysis of Simulated Dataset

1) Simulation Data Generation

First, we evaluated the effectiveness of the RandCon method using a simulated dataset. The *osl-dynamics* toolkit⁴⁸ was employed to generate simulated fMRI time series, utilizing a hidden Markov model that posits the brain is in a particular state at each time point. First, we use a random algorithm to generate states as “ground truth”. To establish certain group relationships between ROIs, we group all ROIs into some sub networks. Each sub network consists of 10 ROIs, as shown in Figure 3, where the smallest grid represents one sub network. For the 10 ROIs within each sub network, we maintain a completely consistent synchronization relationship at all times. For the relationships between sub networks, we set them randomly, allowing them to be completely negative correlation (correlation coefficient is equal to -1), no correlation (0), and completely positive correlation (1). In the *osl-dynamics* simulations, the duration of each state was determined by a Gamma distribution with a shape parameter and a scale parameter. The shape parameter were set as 10 separately in this study, and the scale parameter is set to 5 in other experiments and changed in section 2.5. Upon reaching the predetermined duration, state transitions occur with equal probability to any other state, ensuring a relatively uniform temporal distribution of all states. For each combination of parameters (latent states, number of TRs, number of ROIs, scale parameter in Gamma distribution), data for 600 subjects were generated as a dataset. Within each dataset, the ground truth of latent states remained consistent across these 600 subjects. Figure 3 displays the four states generated by *osl-dynamics* toolkit, along with the time series for the first subject, showing the state at each time point.

2) Validation of robustness

In the simulated data experiments, we compared the performance of four methods: MTD, phase synchronization, sliding window, and RandCon. The MTD method was implemented as described in the original paper²⁵, using the provided code. After obtaining the functional connectivity matrix at each time point, a moving average was applied, with the window size and step length consistent with those used in the sliding window and RandCon methods. The phase synchronization method followed the approach by Yaesoubi et al.⁴⁹, which involves

performing a Hilbert transform on the BOLD signal and calculating the functional connectivity matrix using the instantaneous phase. The sliding window method employed the classic approach²⁰, where a segment of the signal within the window is extracted, and the Pearson correlation is calculated to obtain the functional connectivity matrix. The RandCon method derived the functional connectivity matrix using formula (2), further details are provided in the Methods section. In all experiments conducted in this paper, the convolution kernel parameters of the RandCon model are determined by random sampling. Specifically, each parameter of each convolution kernel is sampled uniformly from a standard Gaussian distribution, and these sampled values are used as the parameters without further training or adjustment.

We added noise to the BOLD sequences generated from the simulated data, then input the noisy BOLD signals into each model. For each dataset, the 600 subjects were randomly divided into 30 groups, each containing 20 subjects. We aggregated all the functional connectivity matrices of the 20 subjects within each group, resulting in a combined input of $(20 * \text{time points/number of windows}) * \text{ROIs} * \text{ROIs}$. For each input, we performed K-means clustering 100 times, with each clustering undergoing 20 iterations. From these 100 times of clustering, we identified the best clustering result using the Davies-Bouldin Index⁵⁰ as the evaluation criterion, and compared the extracted state matrices and state time series with the ground truth from the simulated data.

2.1) Robustness Against Noise

We generated a dataset using a specific combination of parameters. The parameters we selected are 4 latent states, 90 Regions of Interest (ROIs), 1200 Time Points (TRs), and scale parameter is equal to 5. We introduced varying levels of Gaussian white noise into this dataset and assessed each model's resistance to noise. The noise had a mean of 0, with the standard deviation indicating noise intensity. In our experiments, the standard deviation of the noise varied from 0.4 to 1.0, increasing by 0.1 increments. At each noise level, we compare the results of the four models using four metrics: Adjusted Rand Index (ARI), Overlap Ratio, Mean Squared Error (MSE), and Cosine Similarity. The first two metrics assess the fit in the temporal dimension, while the latter two assess the fit in the spatial dimension. The introduction and calculation methods for all metrics can be found in Section C: Measurement Metrics. We calculate these four metrics for each group and average the results across 30 subjects.

2.2) Robustness to ROI numbers

To compare the impact of the number of ROIs on the model's performance, we fixed the noise level at 0.6, and varied the number of ROIs to 30, 60, 90, and 120. The other parameters remained consistent with those specified in Section 2.1. We generated four datasets in total, with each dataset containing 30 groups of subjects, each group consisting of 20 subjects. For each group of subjects, the four methods produced separate results. Our evaluation metrics were the Adjusted Rand Index (ARI) and Cosine Similarity. After obtaining the results, we conducted two-way ANOVA analysis with the Bonferroni correction method to compare whether there were significant differences between RandCon and the other three methods for all 30 groups of subjects under each ROI quantity.

2.3) Robustness to time length

In order to investigate the impact of time length of time series on the four DFC methods, we generated five datasets in total, in each dataset, the number of time points was varied from 400, 600, 800, 1000, and 1200, other parameters remain unchanged with Section 2.1. All

subsequent steps after the dataset generation are consistent with those described in Section 2.2.

2.4) Robustness to Latent States numbers

To investigate the impact of varying the number of hidden states on the outcomes of these four methods, we generated three datasets in total. Other parameters remain unchanged with Section 2.1, we set the number of latent states to 4, 6, and 8. All next steps were consistent with those described in Section 2.2.

2.5) Robustness to State Transition Frequency

The duration of each state is sampled from a Gamma distribution. When the scale parameter of the Gamma distribution changes, the state's duration changes accordingly. A larger scale parameter results in a longer average duration of the state, meaning a lower switching frequency. Other parameters remaining consistent with Section 2.1, we set the scale parameter to 1, 3, 5, and 7, generating four datasets. All subsequent steps were consistent with those described in Section 2.2.

3) Evaluation of the Impact of The Parameters of RandCon Methods

The RandCon model is a simple model characterized by two parameters: the size of the convolution kernel and the number of convolution kernels. The size of the convolution kernel determines the number of time points considered in feature extraction during convolution, while the number of convolution kernels dictates the dimensionality of the extracted features. In the following sections, we will analyze how these two parameters influence the model's performance. We utilized the dataset generated as described in Section 2.1.

3.1) Number of Convolution Kernels

The number of convolution kernels is a key parameter of RandCon, determining the dimensionality increase of the model post-convolution and affecting its noise resistance and robustness. In this experiment, we evaluated the impact of varying the number of convolution kernels on the model's performance using parameters same as Section 2.1, except the noise level of 0.6. Specifically, we tested six different quantities of convolution kernels: {5, 10, 20, 40, 80, 160}, across four noise levels: 0.6, 1.1, 1.6, and 2.6. For each noise level, we conducted experiments with 30 groups, each consisting of 20 subjects. The performance metrics used were ARI and cosine similarity. The resulting will be averaged across all groups.

3.2) Size of Convolution Kernels

In all the above experiments, we used 1×3 convolution kernels. A 1×3 convolution kernel, with a padding length of 1, ensures that the post-convolution signal dimensions match the original signal dimensions, with minimal impact on the model results due to the short padding length. In this experiment, we evaluate the effect of convolution kernel size on the results. Larger convolution kernels can cause discrepancies in signal dimensions post-convolution, and excessive padding can lead to distortion; therefore, we did not use padding in this experiment. We conducted experiments using data with a noise level of 0.6, other parameters same as Section 2.1, comparing only the sliding window method and the RandCon method. We tested six convolution kernel lengths ranging from 4 to 9, with corresponding sliding window lengths also from 4 to 9. We used 30 groups, each consisting of 20 subjects. Due to inconsistencies in time points, we employed the KL divergence of Sojourn Time as the time dimension metric. For the spatial dimension, we used Cosine similarity and MSE. For detailed explanations and calculation methods of these metrics, refer to section C. Measurement Metrics.

B. Real Data Analysis

1) Data Acquisition and Preprocessing

Data Acquisition: The Human Brain Connectome Project (HCP) has publicly released resting-state fMRI data from 1200 healthy subjects (<https://www.humanconnectome.org/>). The rsfMRI data of 100 subjects (age: 22–36 years old, 46 men and 54 women) out of the 1200 subjects were used in this experiment. The HCP ensures the ethics and consent required for the public use of this dataset. Thus, there is no need to obtain further approval from the institutional review board (IRB). All subjects were scanned on a customized 32-channel Siemens 3T “Connectome Skyra” housed at Washington University⁵¹. Each subject underwent two approximately 15-minute resting-state scans, with eyes open and relaxed fixation on a projected bright cross-hair on a dark background. Whole-brain gradient-echo-planar imaging acquisitions were acquired with the following main parameters: repetition time (TR) = 720 ms, echo time (TE) = 33.1 ms, flip angle = 52°, field of view (FOV) = 208×180 mm², matrix = 104×90, slice thickness = 2 mm, number of slices = 72, voxel size = 2×2×2 mm³, multiband factor = 8. In this study, the rs-fMRI data of the “LR” encoded run in the first scan (i.e., REST1) were used. For more information about data acquisition, please refer to the source study.

Preprocessing: The ICA-FIX rs-fMRI data of the HCP that produced the “minimal preprocessing pipelines” and ICA-FIX were used in the study⁵². The minimal preprocessing pipelines included structural and functional pipelines, and ICA-FIX was used as an automatic noise detection algorithm for removing spatial and temporal artifacts such as head motion and physiological noise from fMRI data. We obtained minimally preprocessed R-fMRI data conducted using HCP Functional Pipeline v2.0, involving gradient distortion correction, head motion correction, image distortion correction, and spatial transformation to the Montreal Neurological Institute (MNI) space using one-step spline resampling from the original functional images followed by intensity normalization.

2) ROI Time Course Extraction

90 ROIs were selected based on the anatomical automatic labeling (AAL) atlas⁵³, and their time courses were extracted from the preprocessed rsfMRI data using the python toolbox NiBabel (<https://nipy.org/nibabel/>). Each ROI's time series was normalized to have a mean of 0 and a standard deviation of 1. According to previous studies, these 90 ROIs were divided into nine subnetworks: sensorimotor network (SMN), cingulo-opercular network (CON), auditory network (AUN), default mode network (DMN), visual network (VN), frontoparietal network (FPN), salience network (SN), subcortical network (SCN), and none.

3) Intrinsic Brain State Extraction

For each subject, both the sliding window method and the RandCon method were applied to all the ROIs' time series to extract time-varying functional connectivity patterns. The sliding window method utilized a window of 3 time points with a step size of 1 time point. A functional connectivity matrix with size 90×90 was calculated within each window and a total of 1198 time-varying functional connectivity matrices were obtained for each subject. Moreover, the RandCon method set the convolution kernel width to 3 and the kernel number to 2048, yielding the same number and size of time-varying connectivity matrices as the sliding window method for each subject. Since each connectivity matrix is symmetric, only the lower triangular parts of 1198 matrices of all subjects were used in the following K-means clustering step. The optimal number of clusters was estimated by using the K-means-Elbow method⁵⁴.

Unlike simulated data, real data encompasses greater and more complex inter-subject variability, noise, and various influencing factors⁷. To enhance the stability of the clustering results, we employed a Stacked Denoising Autoencoder (SDAE)⁵⁵ model for dimensionality reduction on the input data of k-means. This model maintained the same learning rate, structure, and embedding dimensions as the original paper. We input the matrices derived from the sliding window method and the RandCon method into the SDAE model separately, training for 200 epochs. The trained model parameters were then used to perform dimensionality reduction on the connectivity matrices, reducing each to 10 dimensions. Subsequently, we applied the K-means clustering method to cluster all time points from all subjects collectively. The Davies-Bouldin Index was used to evaluate the clustering results, identifying the best clustering outcome out of 100 attempts. For each method, this resulted in a sequence of the number of subjects \times number of time points. For each state, we determine the time points in our sequence that correspond to that state and calculate the average FC matrix for these time points. This process yields the average FC patterns for the four states.

4) Temporal and spatial DFC analysis for Sliding windows and RandCon

To investigate the temporal dynamic characteristics of the brain states extracted by the sliding window and the RandCon DFC methods, the mean dwell time and the fraction of time were calculated for each state of each subject. The mean dwell time of state k represents the average number of consecutive windows in which state k was active. The fraction of time of state k indicates the proportion of windows in which state k was active.

Functional Connectivity (FC) Variability and Centroid Similarity were calculated to measure the spatial dynamic characteristics of each subject. For each subject, the FC variability matrix was obtained by calculating the standard deviation of each connection across all sliding windows. The FC variability of each subject was then calculated by averaging the variabilities across all connections in the upper triangle of the FC variability matrix. For Centroid calculation, the Fisher transformation was firstly applied to the connectivity matrices of each subject, and a mean connectivity matrix was obtained by averaging all the time-varying matrices across time points. Then, the cosine similarity between the connectivity matrix at each time point and the mean connectivity matrix was calculated. The average of these cosine similarities provided the average Centroid Similarity for each subject.

C. Measurement Metrics

Adjusted Rand Index (ARI)

The Adjusted Rand Index (ARI)⁵⁶ is an evaluation metric used in clustering analysis to assess the similarity between clustering results and true labels. By accounting for the impact of random matching, this metric ensures that the evaluation of the match between clustering results and true labels is more accurate. The formula for ARI is as follows:

$$ARI = \frac{\sum_{ij} \binom{n_{ij}}{2} - \left[\sum_i \binom{a_i}{2} \sum_j \binom{b_j}{2} \right] / \binom{n}{2}}{\frac{1}{2} \left[\sum_i \binom{a_i}{2} + \sum_j \binom{b_j}{2} \right] - \left[\sum_i \binom{a_i}{2} \sum_j \binom{b_j}{2} \right] / \binom{n}{2}} \quad (4)$$

Here, n represents the total number of samples, n_{ij} denotes the number of samples that

are both in cluster i and in true category j , a_i represents the number of samples in cluster i , and b_j represents the number of samples in true category j . The terms in the formula calculate the match between the clustering results and the true labels. By considering the consistency of all possible pairs of samples and adjusting for the expected consistency, the final Adjusted Rand Index (ARI) is obtained.

Sojourn Time

For time series of a state, we calculate and record the number of consecutive time points for which each state appears, referred to as the dwell time. Consequently, each state has a distribution of dwell times. For the clustering result labels and the true labels of each state, we calculate a distribution and then compute the Kullback-Leibler (KL) divergence between the clustering result distributions and the true label distributions. This measures the similarity of the dwell times of each state between the clustering results and the true scenario. Finally, we calculate the average KL divergence across all states.

Mean Squared Error (MSE)

Since the states and labels obtained by K-means clustering are random, we first calculate the Euclidean distances between all model output states and all true states. We then match the model output states to the true states by minimizing the total distance. Once the matching is completed, we calculate the Mean Squared Error (MSE) between the corresponding states, representing the degree of difference between the two matrices. Specifically, MSE measures the average of the squared differences between corresponding elements of these two matrices. It quantifies the similarity or difference between the two matrices: a smaller value indicates greater similarity, while a larger value indicates greater difference. The formula is as follows:

$$\text{MSE} = \frac{1}{n} \sum_{i=1}^n (A_i - B_i)^2 \quad (5)$$

Here, A and B represent the two states, n is the total number of elements in the states, and A_i and B_i are the elements at the corresponding positions in states A and B.

Finally, we average the MSE values of all states to obtain an overall metric, representing the overall spatial pattern similarity of the clustering for this group of subjects.

Cosine Similarity

Similar to MSE, after matching the states, we calculate the cosine similarity between the corresponding states. The formula is as follows:

$$\text{Cosine Similarity} = \frac{\mathbf{A} \cdot \mathbf{B}}{\|\mathbf{A}\| \|\mathbf{B}\|} = \frac{\sum_{i=1}^n A_i B_i}{\sqrt{\sum_{i=1}^n A_i^2} \sqrt{\sum_{i=1}^n B_i^2}} \quad (6)$$

Here, A and B represent the two states, n is the total number of elements in the states, and A_i and B_i are the elements at the corresponding positions in states A and B.

Finally, we average the cosine similarity values of all states to obtain an overall metric, representing the overall spatial pattern similarity of the clustering for this group of subjects.

References

1. Fox, M. D. & Raichle, M. E. Spontaneous fluctuations in brain activity observed with functional magnetic resonance imaging. *Nat Rev Neurosci* **8**, 700–711 (2007).
2. Smith, S. M. *et al.* Functional connectomics from resting-state fMRI. *Trends in Cognitive Sciences* **17**, 666–682 (2013).
3. Sakoğlu, Ü. *et al.* A method for evaluating dynamic functional network connectivity and task-modulation: application to schizophrenia. *Magn Reson Mater Phy* **23**, 351–366 (2010).
4. Chang, C. & Glover, G. H. Time–frequency dynamics of resting-state brain connectivity measured with fMRI. *NeuroImage* **50**, 81–98 (2010).
5. Hutchison, R. M. *et al.* Dynamic functional connectivity: Promise, issues, and interpretations. *NeuroImage* **80**, 360–378 (2013).
6. Preti, M. G., Bolton, T. A. & Van De Ville, D. The dynamic functional connectome: State-of-the-art and perspectives. *NeuroImage* **160**, 41–54 (2017).
7. Lurie, D. J. *et al.* Questions and controversies in the study of time-varying functional connectivity in resting fMRI. *Network Neuroscience* **4**, 30–69 (2020).
8. Calhoun, V. D., Miller, R., Pearlson, G. & Adalı, T. The Chronnectome: Time-Varying Connectivity Networks as the Next Frontier in fMRI Data Discovery. *Neuron* **84**, 262–274 (2014).
9. Zhang, W. *et al.* Abnormal dynamic functional connectivity between speech and auditory areas in schizophrenia patients with auditory hallucinations. *NeuroImage: Clinical* **19**, 918–924 (2018).
10. Hellyer, P. J., Scott, G., Shanahan, M., Sharp, D. J. & Leech, R. Cognitive Flexibility through Metastable Neural Dynamics Is Disrupted by Damage to the Structural Connectome. *Journal*

of Neuroscience **35**, 9050–9063 (2015).

11. Chyl, K., Fraga-González, G., Brem, S. & Jednoróg, K. Brain dynamics of (a)typical reading development—a review of longitudinal studies. *npj Sci. Learn.* **6**, 4 (2021).
12. Erb, J., Henry, M. J., Eisner, F. & Obleser, J. The Brain Dynamics of Rapid Perceptual Adaptation to Adverse Listening Conditions. *Journal of Neuroscience* **33**, 10688–10697 (2013).
13. White, E. J. *et al.* Addressing the Language Binding Problem With Dynamic Functional Connectivity During Meaningful Spoken Language Comprehension. *Front. Psychol.* **9**, 1960 (2018).
14. Engels, G., Vlaar, A., McCoy, B., Scherder, E. & Douw, L. Dynamic Functional Connectivity and Symptoms of Parkinson’s Disease: A Resting-State fMRI Study. *Front. Aging Neurosci.* **10**, 388 (2018).
15. Wang, L. *et al.* Dynamic functional reorganization of the motor execution network after stroke. *Brain* **133**, 1224–1238 (2010).
16. Rabany, L. *et al.* Dynamic functional connectivity in schizophrenia and autism spectrum disorder: Convergence, divergence and classification. *NeuroImage: Clinical* **24**, 101966 (2019).
17. Sun, Y. *et al.* Brain state-dependent dynamic functional connectivity patterns in attention-deficit/hyperactivity disorder. *Journal of Psychiatric Research* **138**, 569–575 (2021).
18. Wang, X.-H., Jiao, Y. & Li, L. Identifying individuals with attention deficit hyperactivity disorder based on temporal variability of dynamic functional connectivity. *Sci Rep* **8**, 11789 (2018).
19. Li, Y. *et al.* Dynamic Functional Connectivity Reveals Abnormal Variability and Hyper-connected Pattern in Autism Spectrum Disorder. *Autism Research* **13**, 230–243 (2020).

20. Allen, E. A. *et al.* Tracking Whole-Brain Connectivity Dynamics in the Resting State. *Cerebral Cortex* **24**, 663–676 (2014).
21. Thompson, W. H. & Fransson, P. The frequency dimension of fMRI dynamic connectivity: Network connectivity, functional hubs and integration in the resting brain. *NeuroImage* **121**, 227–242 (2015).
22. Vidaurre, D., Smith, S. M. & Woolrich, M. W. Brain network dynamics are hierarchically organized in time. *Proc. Natl. Acad. Sci. U.S.A.* **114**, 12827–12832 (2017).
23. Long, Z. *et al.* Improved dynamic functional connectivity estimation with an alternating hidden Markov model. *Cogn Neurodyn* (2022) doi:10.1007/s11571-022-09874-3.
24. Zhang, G. *et al.* Estimating Dynamic Functional Brain Connectivity With a Sparse Hidden Markov Model. *IEEE Trans. Med. Imaging* **39**, 488–498 (2020).
25. Shine, J. M. *et al.* Estimation of dynamic functional connectivity using Multiplication of Temporal Derivatives. *NeuroImage* **122**, 399–407 (2015).
26. Broumand, A., Esfahani, M. S., Yoon, B.-J. & Dougherty, E. R. Discrete optimal Bayesian classification with error-conditioned sequential sampling. *Pattern Recognition* **48**, 3766–3782 (2015).
27. Cribben, I., Haraldsdottir, R., Atlas, L. Y., Wager, T. D. & Lindquist, M. A. Dynamic connectivity regression: Determining state-related changes in brain connectivity. *NeuroImage* **61**, 907–920 (2012).
28. Lindquist, M. A., Xu, Y., Nebel, M. B. & Caffo, B. S. Evaluating dynamic bivariate correlations in resting-state fMRI: A comparison study and a new approach. *NeuroImage* **101**, 531–546 (2014).

29. Mokhtari, F., Akhlaghi, M. I., Simpson, S. L., Wu, G. & Laurienti, P. J. Sliding window correlation analysis: Modulating window shape for dynamic brain connectivity in resting state. *NeuroImage* **189**, 655–666 (2019).
30. Rashid, B., Damaraju, E., Pearlson, G. D. & Calhoun, V. D. Dynamic connectivity states estimated from resting fMRI Identify differences among Schizophrenia, bipolar disorder, and healthy control subjects. *Front. Hum. Neurosci.* **8**, (2014).
31. Hindriks, R. *et al.* Can sliding-window correlations reveal dynamic functional connectivity in resting-state fMRI? *NeuroImage* **127**, 242–256 (2016).
32. Leonardi, N. & Van De Ville, D. On spurious and real fluctuations of dynamic functional connectivity during rest. *NeuroImage* **104**, 430–436 (2015).
33. Savva, A. D., Mitsis, G. D. & Matsopoulos, G. K. Assessment of dynamic functional connectivity in resting-state fMRI using the sliding window technique. *Brain and Behavior* **9**, e01255 (2019).
34. Zhuang, X. *et al.* Single-scale time-dependent window-sizes in sliding-window dynamic functional connectivity analysis: A validation study. *NeuroImage* **220**, 117111 (2020).
35. Espinoza, F. A. *et al.* Characterizing Whole Brain Temporal Variation of Functional Connectivity via Zero and First Order Derivatives of Sliding Window Correlations. *Front. Neurosci.* **13**, 634 (2019).
36. Vergara, V. M., Abrol, A. & Calhoun, V. D. An average sliding window correlation method for dynamic functional connectivity. *Human Brain Mapping* **40**, 2089–2103 (2019).
37. Li, Z., Liu, F., Yang, W., Peng, S. & Zhou, J. A Survey of Convolutional Neural Networks: Analysis, Applications, and Prospects. *IEEE Trans. Neural Netw. Learning Syst.* **33**, 6999–7019

(2022).

38. Kiranyaz, S., Ince, T., Abdeljaber, O., Avci, O. & Gabbouj, M. 1-D Convolutional Neural Networks for Signal Processing Applications. in *ICASSP 2019 - 2019 IEEE International Conference on Acoustics, Speech and Signal Processing (ICASSP)* 8360–8364 (IEEE, Brighton, United Kingdom, 2019). doi:10.1109/ICASSP.2019.8682194.
39. Naranjo-Torres, J. *et al.* A Review of Convolutional Neural Network Applied to Fruit Image Processing. *Applied Sciences* **10**, 3443 (2020).
40. Murray-Smith, D. J., Kocijan, J. & Gong, M. A signal convolution method for estimation of controller parameter sensitivity functions for tuning of feedback control systems by an iterative process. *Control Engineering Practice* **11**, 1087–1094 (2003).
41. Greene, A. S., Horien, C., Barson, D., Scheinost, D. & Constable, R. T. Why is everyone talking about brain state? *Trends in Neurosciences* **46**, 508–524 (2023).
42. Zhu, W. *et al.* Aberrant Functional Connectivity of Sensorimotor Network and Its Relationship With Executive Dysfunction in Bipolar Disorder Type I. *Front. Neurosci.* **15**, 823550 (2022).
43. Gratton, C., Sun, H. & Petersen, S. E. Control networks and hubs. *Psychophysiol* **55**, e13032 (2018).
44. Denkova, E., Nomi, J. S., Uddin, L. Q. & Jha, A. P. Dynamic brain network configurations during rest and an attention task with frequent occurrence of mind wandering. *Hum Brain Mapp* **40**, 4564–4576 (2019).
45. Xu, Y. *et al.* Altered Dynamic Functional Connectivity in Subcortical Ischemic Vascular Disease With Cognitive Impairment. *Front. Aging Neurosci.* **13**, 758137 (2021).
46. Koshiyama, D. *et al.* Role of subcortical structures on cognitive and social function in

- schizophrenia. *Sci Rep* **8**, 1183 (2018).
47. de Lacy, N., McCauley, E., Kutz, J. N. & Calhoun, V. D. Sex-related differences in intrinsic brain dynamism and their neurocognitive correlates. *NeuroImage* **202**, 116116 (2019).
 48. Gohil, C. *et al.* osl-dynamics, a toolbox for modeling fast dynamic brain activity. *eLife* **12**, RP91949 (2024).
 49. Yaesoubi, M., Allen, E. A., Miller, R. L. & Calhoun, V. D. Dynamic coherence analysis of resting fMRI data to jointly capture state-based phase, frequency, and time-domain information. *NeuroImage* **120**, 133–142 (2015).
 50. Davies, D. L. & Bouldin, D. W. A Cluster Separation Measure. *IEEE Trans. Pattern Anal. Mach. Intell.* **PAMI-1**, 224–227 (1979).
 51. Van Essen, D. C. *et al.* The WU-Minn Human Connectome Project: An overview. *NeuroImage* **80**, 62–79 (2013).
 52. Glasser, M. F. *et al.* The minimal preprocessing pipelines for the Human Connectome Project. *NeuroImage* **80**, 105–124 (2013).
 53. Rolls, E. T., Huang, C.-C., Lin, C.-P., Feng, J. & Joliot, M. Automated anatomical labelling atlas 3. *NeuroImage* **206**, 116189 (2020).
 54. Syakur, M. A., Khotimah, B. K., Rochman, E. M. S. & Satoto, B. D. Integration K-Means Clustering Method and Elbow Method For Identification of The Best Customer Profile Cluster. *IOP Conf. Ser.: Mater. Sci. Eng.* **336**, 012017 (2018).
 55. Vincent, P., Larochelle, H., Lajoie, I., Bengio, Y. & Manzagol, P.-A. Stacked Denoising Autoencoders: Learning Useful Representations in a Deep Network with a Local Denoising Criterion.

56. Santos, J. M. & Embrechts, M. On the Use of the Adjusted Rand Index as a Metric for Evaluating Supervised Classification. in *Artificial Neural Networks – ICANN 2009* (eds. Alippi, C., Polycarpou, M., Panayiotou, C. & Ellinas, G.) vol. 5769 175–184 (Springer Berlin Heidelberg, Berlin, Heidelberg, 2009).

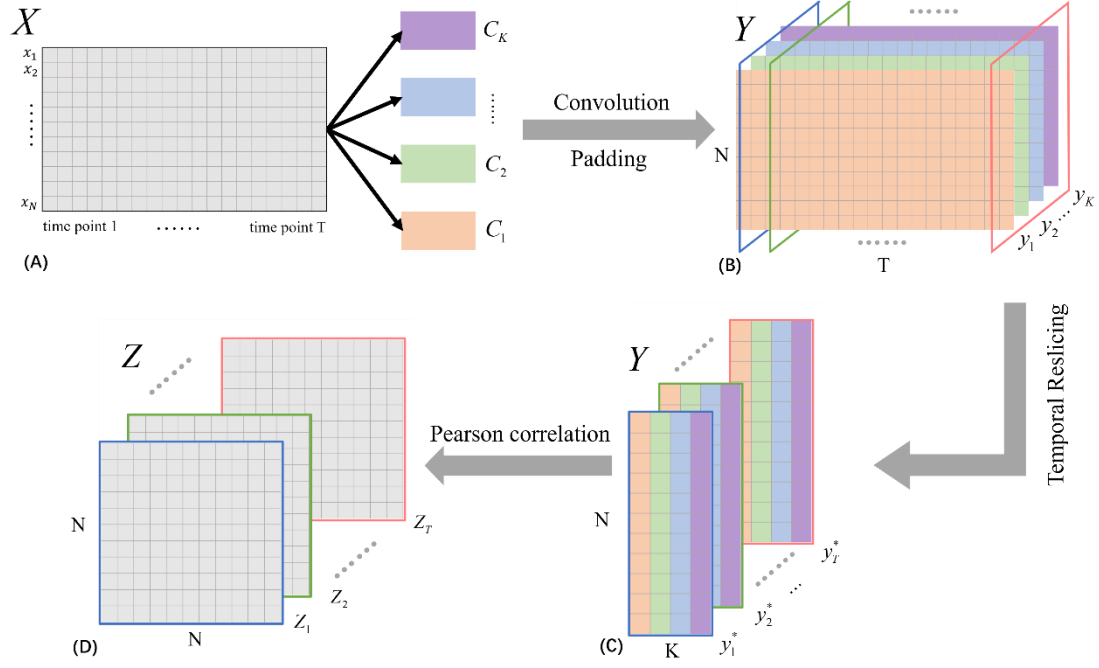


Fig. 1 Overall flowchart of the RandCon model. (A) The time series data from a single subject. (B) A multi-dimensional time series obtained after convolutional upscaling, where P_k corresponds to a feature map derived from filtering the original series using convolution kernel k . (C) The sequence after temporal reslicing, with Q_t representing the multi-dimensional features of all ROIs at a specific time point. (D) Model results, where Z_t represents the functional connectivity matrix at a specific time point.

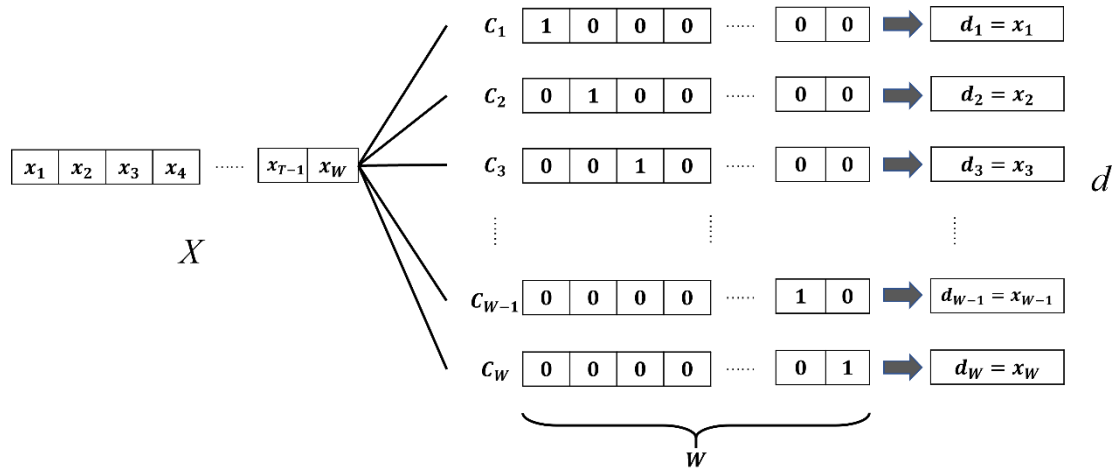


Fig.2 Using a special convolution kernel produces the same results as the sliding window method, demonstrating that the sliding window method is a special case of multi-dimensional convolution.

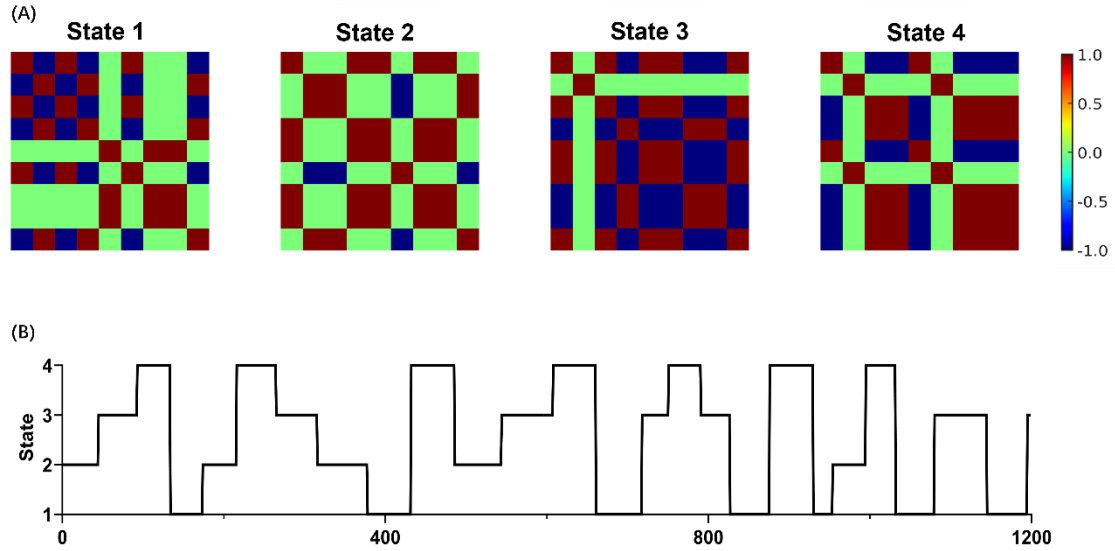


Fig.3 Simulated data generated using osl-dynamics, along with the state sequences of the first subject. (A) Generated ground truth examples of the four states. (B) State time series example of the states for the first subject.

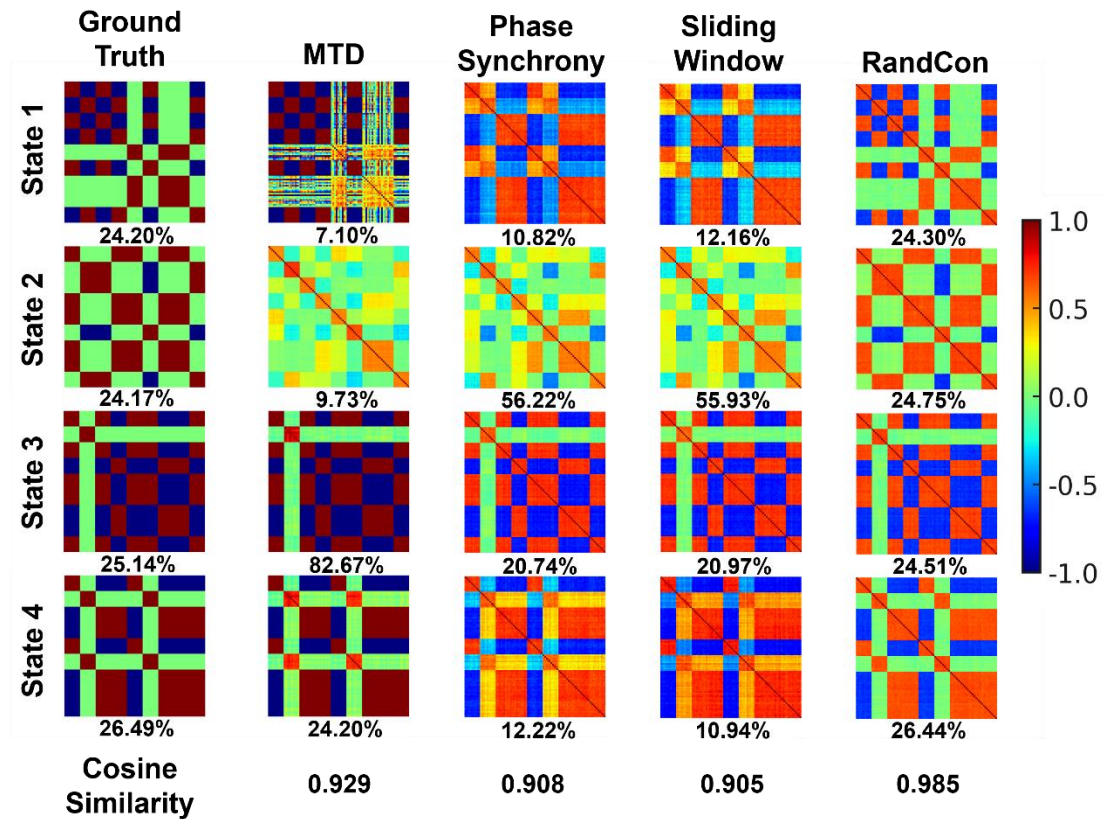


Fig.4 The four states of ground truth and the results of state fitting using four different models, along with cosine similarity and the proportion of time spent in each state. The data utilized includes the results from the first group of 30 subjects, with a noise standard deviation of 0.6, 90 ROIs, 1200 TRs, and a scale parameter of 5.

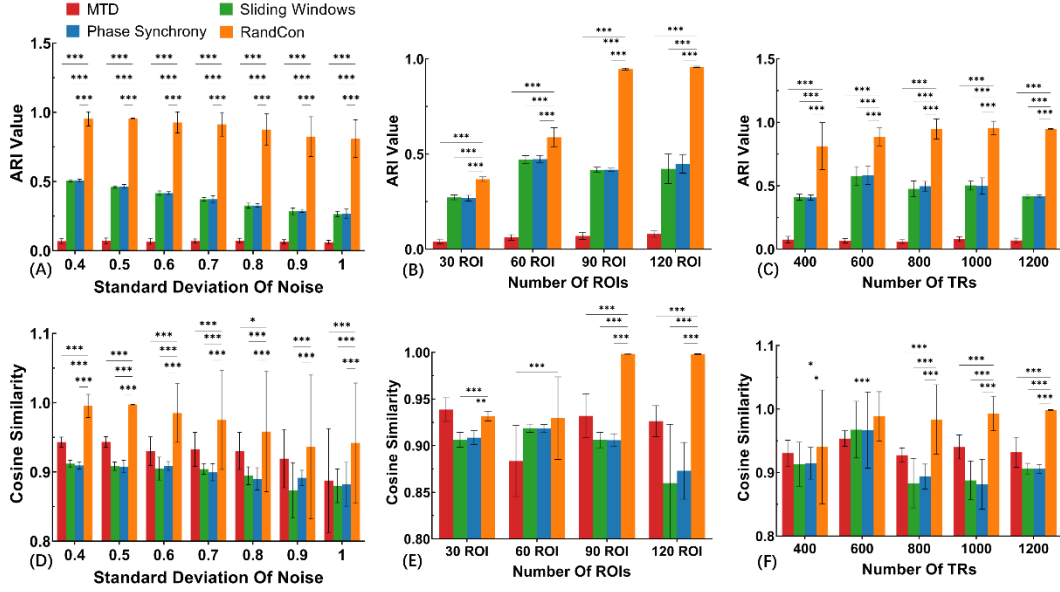


Fig.5 Validation results of simulated data under different noise levels, numbers of ROIs, and numbers of TRs, including ARI values in the temporal dimension and cosine similarity in the spatial dimension. (A) (D) ARI and cosine similarity results from Section 2.1. (B) (E) ARI and cosine similarity results from Section 2.2. (C) (F) ARI and cosine similarity results from Section 2.3. The figure exclusively presents the significance results of the RandCon method in comparison to the other three models; it does not display the significance test results within the other three models themselves. (* for $P < 0.05$, ** for $P < 0.01$, *** for $P < 0.001$)

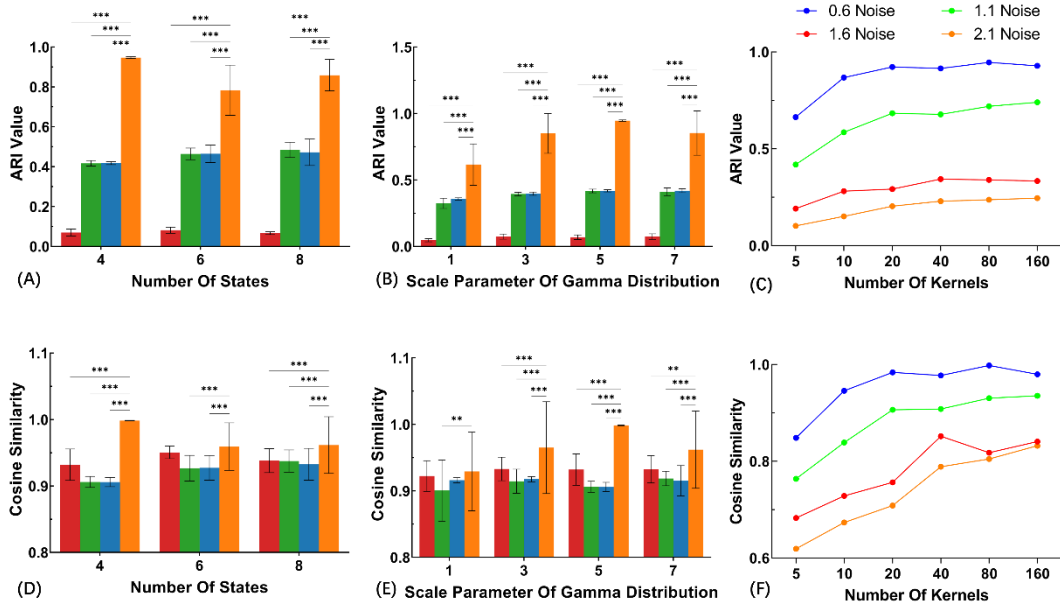


Fig.6 Experimental results on simulated data with varying numbers of states, different state transition frequencies, and different numbers of convolution kernels. (A) (D) ARI and cosine similarity results from Section 2.4. (B) (E) ARI and cosine similarity results from Section 2.5. (C) (F) ARI and cosine similarity results from Section 2.6. The figure exclusively presents the significance results of the RandCon method in comparison to the other three models; it does not display the significance test results within the other three models themselves. (* for $P < 0.05$, ** for $P < 0.01$, *** for $P < 0.001$)

(F) ARI and cosine similarity results from Section 3.1. The figure exclusively presents the significance results of the RandCon method in comparison to the other three models; it does not display the significance test results within the other three models themselves. (* for $P<0.05$, ** for $P<0.01$, *** for $P<0.001$)

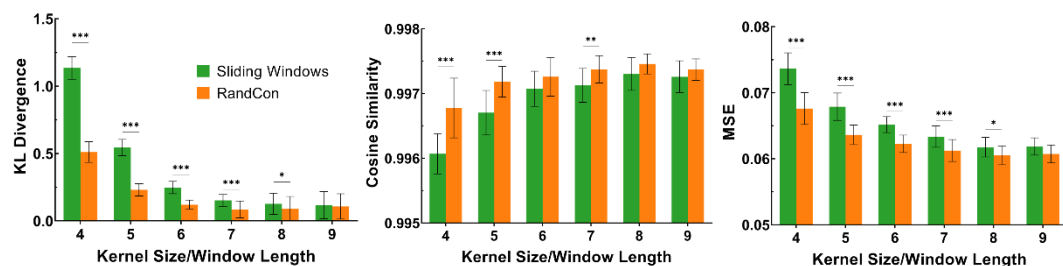


Fig.7 The impact of different convolution kernel sizes and window lengths on the results. The temporal dimension metric is the KL divergence of sojourn time, while the spatial dimension metrics are cosine similarity and MSE values. (* for $P<0.05$, ** for $P<0.01$, *** for $P<0.001$)

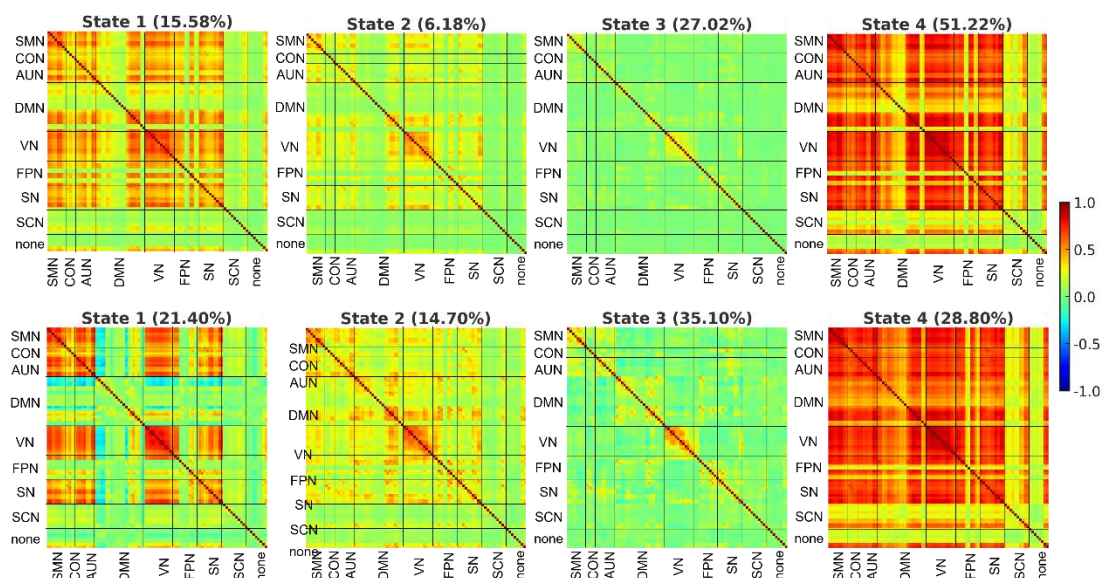


Fig.8 The four states extracted from real data of one hundred subjects using the RandCon method and the sliding window method, respectively.

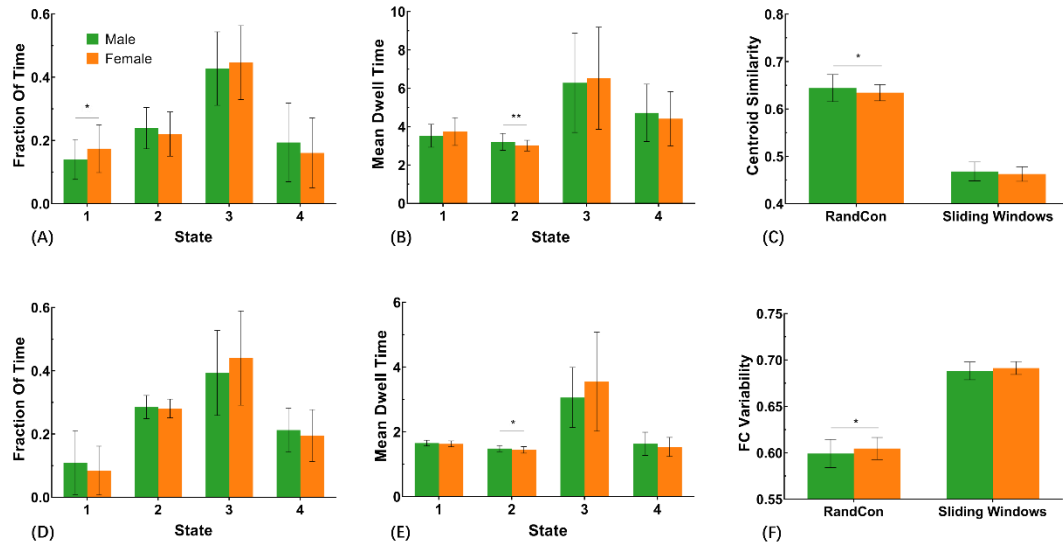


Fig.9 Experimental results on real data, including the metrics of fraction of time and mean dwell time in the temporal dimension, and centroid similarity and functional connectivity variability in the spatial dimension. (A) (B) The results of the proportion of time, mean dwell time, and cosine similarity obtained by the RandCon method on real data for male and female participants. (D) (E) The results obtained by the sliding window method using the same metrics. (C) Comparison of the centroid similarity obtained by the two methods on different gender subjects. (F) Comparison of the FC variability obtained by the two methods on different gender subjects. (* for $P < 0.05$, ** for $P < 0.01$, *** for $P < 0.001$)